Use of phase-locking in four-wave Raman mixing for generating ultrashort optical pulses

Hiroyuki Kawano, Tomonori Mori, Yasuyuki Hirakawa, and Totaro Imasaka*
Department of Chemical Science and Technology, Faculty of Engineering, Kyushu University, Hakozaki, Fukuoka 812, Japan
(Received 19 June 1998)

The intensities of high-order rotational Raman lines are calculated by computer simulation in the approximation of time-independent plane-wave pumping based on the currently accepted model used in studies of four-wave Raman mixing (FWRM). When the phases of the rotational lines are assumed to be slightly random, the intensities are drastically decreased. Such reduction in intensity becomes more serious with increasing phase distortion, indicating that the emission lines generated by FWRM requiring phase matching are coherently phased. In other words, phase matching is equivalent to phase locking or mode locking in FWRM. These results suggest that FWRM has potential for use in generating ultrashort optical pulses shorter than 1 fs. [S1050-2947(99)03206-0]

PACS number(s): 42.65.Dr

I. INTRODUCTION

The recently developed lasers which produce ultrashort optical pulses have a variety of basic and industrial applications, such as studies of nonlinear spectroscopy and telecommunication. The generation of 6-fs pulses was reported in 1987 [1], in which a white light continuum produced by self-phase modulation (SPM) in an optical fiber was compressed by grating and prism pairs with negative group velocity dispersions (GVDs) [2]. This approach, which is referred to as a pulse compression technique, is frequently employed in the generation of femtosecond optical pulses. No significant improvement has, however, been reported since that time, although the generation of 5-fs pulses was reported by several groups in 1997 [3,4]. There are two major difficulties in the generation of yet shorter optical pulses. (1) A wide frequency domain is required for the generation of ultrashort optical pulses, as is evident from the uncertainty principle. The expansion of the frequency domain by SPM, however, has practical limitations. (2) It is difficult to completely compensate for high-order phase distortion induced by optical elements by means of optics such as a prism pair in the subfemtosecond regime.

Recently, several groups have proposed the use of high-order harmonics because of their wide frequency domain, which extends from the visible to the soft x ray [5–9]. Unfortunately, the conversion efficiency is rather small, especially for higher-order harmonics which form a plateau region, and, as a result, it may be difficult to generate a strong ultrashort optical pulse by Fourier synthesis of the obtained emission lines. One suggestion to overcome this problem involves the removal of the fundamental and low-order harmonics by a metal filter. This approach, however, reduces the total pulse energy, making the generation of the high-intensity optical pulse difficult. It has also been pointed out that the phase difference between two harmonics is completely random in the plateau region, which is related to the ionization potential and the ponderomotive energy of the medium (neon) used [9].

An alternative method has been proposed [10], which utilizes the Fourier synthesis of multiple stimulated Raman emission generated in hydrogen gas. It is known that numerous Raman lines are simultaneously generated by stimulated Raman scattering (SRS) and the succeeding four-wave Raman mixing (FWRM). When vibrational lines ($v=0$, $J=1 \rightarrow v=1$, $J=1$) generated in hydrogen are used as Fourier components under the assumptions that all the Raman components are properly phased and are forced to propagate with the same group velocity in the plane-wave approximation, highly repetitive pulses separated by 8 fs are produced because of a considerably large vibrational Raman shift frequency (4155 cm^{-1}) [10]. It is also reported that multifrequency 2π solitons occurring in the cascade-stimulated Raman scattering propagate with the same group velocity and are phase locked to each other [11,12]. The separation of the pulses (8 fs) may, however, be too small for most practical applications.

On the other hand, numerous rotational lines are generated by using a two-color or elliptically polarized pump beam [13–15]. The Raman shift frequency for the rotational transition ($v=0$, $J=1 \rightarrow v=0$, $J=3$) is 587 cm^{-1}, thus producing repetitive pulses separated by 57 fs. This value is more realistic for the generation of ultrashort optical pulses and for measurements of the pulse width. We have already reported that more than 40 rotational Raman lines are generated by using a picosecond and femtosecond Ti:sapphire laser [16–18] and a femtosecond KrF excimer laser [19] as a pump source and hydrogen gas as the Raman medium. The pulse duration calculated by Fourier synthesis of the emission lines is reported to be 0.4 fs.

For the generation of ultrashort optical pulses by Fourier synthesis, all the emission lines are assumed to be phase locked. It is well known that the emission lines generated by FWRM are ''phase matched'' as written by

$$2n_{\text{pump}}\mathbf{k}_{\text{pump}} = n_{\text{seed}}\mathbf{k}_{\text{seed}} + n_{\text{signal}}\mathbf{k}_{\text{signal}}, \tag{1}$$

where $\mathbf{k}_{\text{pump}}$, $\mathbf{k}_{\text{seed}}$, and $\mathbf{k}_{\text{signal}}$ are the wave vectors for the pump beam, the seed (Stokes) beam, and the signal beam

*FAX: 81-92-632-5209.
Electronic address: imasaka@cstf.kyushu-u.ac.jp

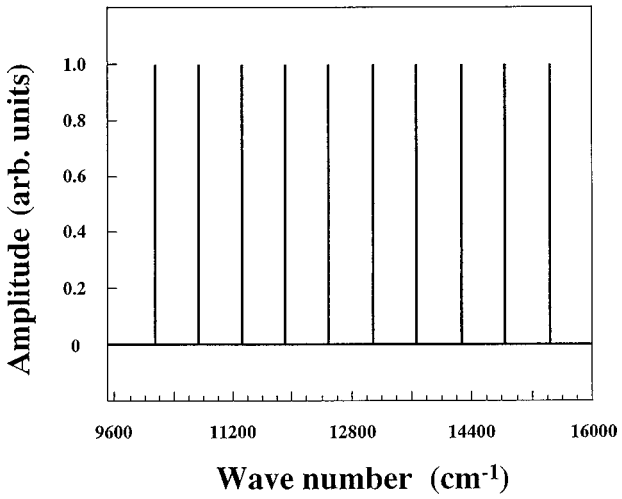

FIG. 1. Spectral profile used in Fourier synthesis of multifrequency laser emission. The emission lines are assumed to have equal intensities (amplitude), and a frequency separation of 587 cm^{-1} which corresponds to the energy of rotational transition from $v=0$, $J=1$ to $v=0$, $J=3$ for hydrogen.

(e.g., the anti-Stokes or the second Stokes generated), respectively, and n_{pump}, n_{seed}, and n_{signal} are the refractive indices of the Raman medium at the wavelengths of the pump, seed, and signal beams, respectively. This equation predicts that the time for traveling a specified distance for $2\mathbf{k}_{\text{pump}}$, i.e., the sum of the wave vectors for the pump beams would be identical to that for $\mathbf{k}_{\text{seed}}+\mathbf{k}_{\text{signal}}$, i.e., the sum of the wave vectors for the seed and the signal beams. This phase-matching requirement has already been experimentally verified: a ring-shaped pattern has been observed for the anti-Stokes beam due to a small phase mismatching [20–22]. The speeds of light are different for these emissions, since the refractive indices are different at the respective emission lines. As a result, Eq. (1) is valid only when the refractive index changes in a linear manner against the frequency of light in the Raman medium. Hydrogen gas is almost (but not completely) the case and explains why a ring shape is observed for the anti-Stokes beam. Thus this phenomenon strongly suggests that all the ''phases'' of the waves would be ''matched.'' However, it provides no further explicit evidence concerning the relationship between the phases of the emissions generated by FWRM.

When numerous equally spaced emission lines are generated by FWRM and are exactly phase locked, a subfemtosecond optical pulse can be generated. Since a wide frequency domain, i.e., from the far-ultraviolet to the near-infrared region, is involved in the generation of a subfemtosecond pulse, GVD may not always be negligible, even for the case of hydrogen gas used as a Raman medium. Thus, phase distortion must be correctly compensated in order to generate ultrashort pulses. The magnitude of the phase distortion in hydrogen, however, has not yet been discussed in detail.

In this paper, we report on two subjects. (1) The emissions generated by FWRM are phase locked. This is verified by computer simulation based on the model currently used in studies of FWRM for the generation of high-order Raman lines. In other words, phase matching is equivalent to phase

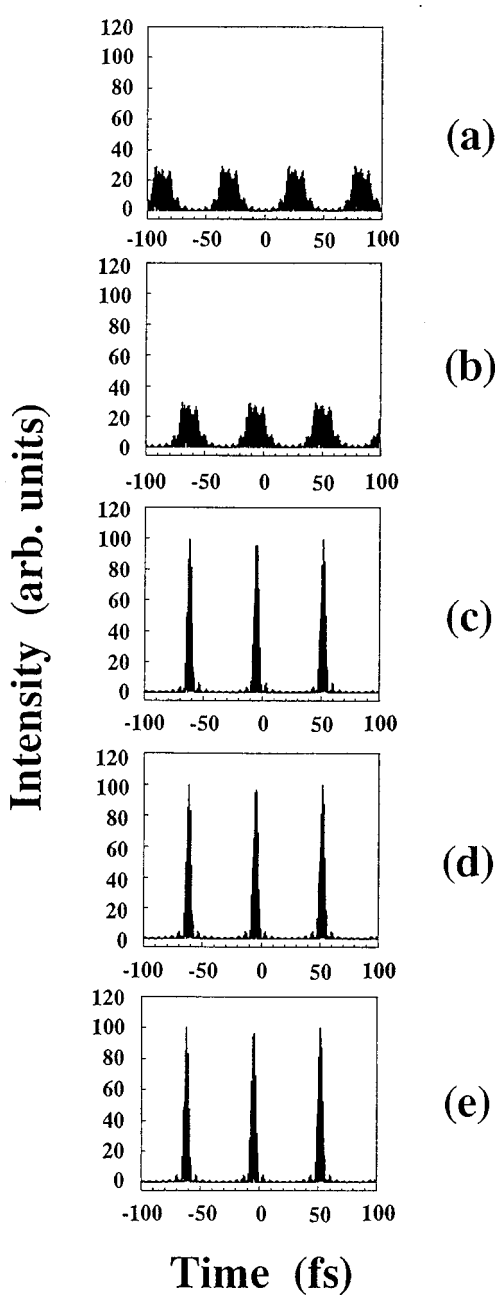

FIG. 2. Laser pulse train calculated by Fourier synthesis of the Raman lines indicated in Fig. 1. All Raman emissions are assumed to be phase locked at the focal point ($z=0$) and to travel 3 m prior to detection. Phase distortion compensation; (a) none, (b) first order only, (c)first to second orders, (d) first to third orders, (e) total distortions.

locking or mode locking in FWRM. (2) Ultrashort optical pulses can be generated by compensating the second-order dispersion in hydrogen because of the low density (small dispersion), which is in contrast to the case of solid optics with high densities (large dispersion). Since the wavelength region of the rotational lines already generated by FWRM extends over a range of more than 700 nm (239–993 nm), which is capable of generating laser pulses of 0.4 fs [17,18], these results strongly suggest the potential advantage of FWRM in the generation of ultrashort optical pulses which might break the 1-fs barrier.

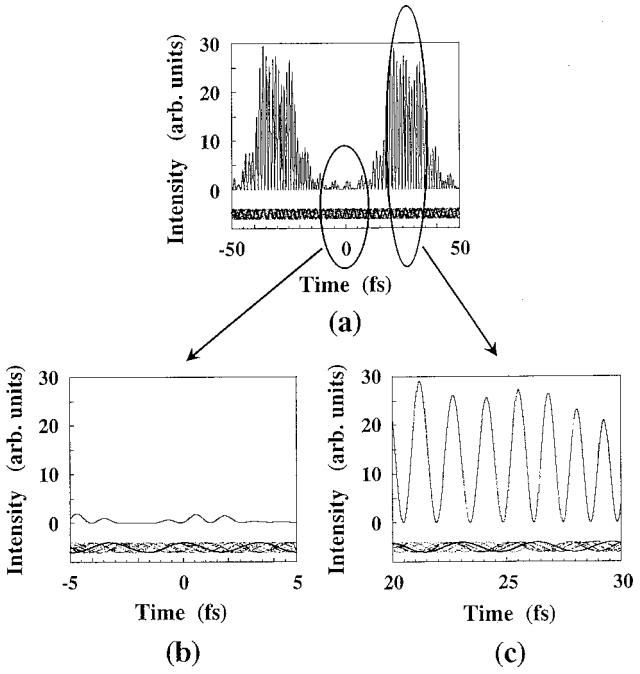

FIG. 3. Magnified views of the laser pulse train indicated in Fig. 2(a). (b) and (c) are expanded views of the baseline and peak parts in (a), respectively. Ten waves (fundamental and nine Raman components) are drawn below the synthesized wave.

II. THEORY

The total electric field consisting of all the frequency components generated by SRS and FWRM, $E(z)$, can be expressed by

$$E(z)=\sum_j E_j(z)\exp[-i(k_jz-\omega_jt)] \times\exp\{-i[n(\omega_j)-1]k_jz\}, \tag{2}$$

where $E_j(z)$ is the electric field for the jth component at distance z ($j=-1,-2,\ldots$ for the Stokes, 0 for the fundamental, $+1$, $+2,\ldots$ for the anti-Stokes components), $k_j=\omega_j/c$ is the wave vector where ω_j is the angular frequency and c is the velocity of light in the vacuum, t is the time, and $n(\omega_j)$ is the refractive index of the medium where $\omega_j=\omega_f+j\omega_R:\omega_f$ and ω_R are the angular frequency of the fundamental beam and the Raman shift frequency, respectively. The first exponential term represents the propagation of the wave in the vacuum and the second term originates from the phase shift induced by the dispersion of the medium. In this study, a series of coupled complex differential equations are assumed to describe the respective SRS or FWRM emissions propagating in the z direction as [21,22]

$$\frac{\partial E_j}{\partial z}=\sum_m \omega_j g_{m,j+1}C_{j,m}E_{j+1}E_m^*E_{m-1}\exp(i\Delta_{m,j+1}z) -\sum_m \omega_j g_{m,j}C_{j-1,m}E_{j-1}E_mE_{m-1}^*\exp(-\Delta_{m,j}z), \tag{3}$$

where g is the gain, and the superscript ''*'' denotes the complex conjugate. In this study, a time-independent treatment is used to simplify the calculation by assuming that the pulse width of the fundamental beam is sufficiently long (essentially a continuous wave). Therefore, temporal separation of the pump and generated pulses arising from a beam walkoff induced by dispersion of a Raman medium is neglected. This assumption is valid for long pulses (>1 ps). In other words, this walkoff effect is no longer negligible for pulses shorter than 1 ps. For such short pulses, the efficiency for the generation of the rotational lines is much less than that predicted from the theory. This point is not discussed in detail in this study, because the discussion of the absolute efficiency is not the subject of this study. In the above equation, the collisional term, i.e., $\exp\{-(t-t')/T_2\}$, in the original paper is neglected, since the time domain concerned in this study (less than several picoseconds) is much shorter than the dephasing time T_2 (several hundred picoseconds for 10 atm of hydrogen). The effect of dispersion is taken into account in the exponential terms. The parameter Δ is given by

$$\Delta_{m,j}=\Delta_m-\Delta_j, \tag{4a}$$

TABLE I. Phase delay of stimulated Raman emission. S: Stokes component. AS: Anti-Stokes component. d: Phase delay; the delay for wave transmission in hydrogen from that in vacuum. c.d.: Compensated phase delay. r.d.: Residual phase delay (r.d.=d-c.d.). Unit: radian.

Raman emission	First order			Second order		Third order	
	d	c.d.	r.d.	c.d.	r.d.	c.d.	r.d.
S4	884.3	882.0	2.1450	884.4	−0.1025	884.4	−0.0092
S3	936.9	936.0	0.8674	936.9	0.0148	936.9	−0.0103
S2	989.7	989.9	−0.1650	989.7	0.0694	989.7	−0.0105
S1	1043.0	1044.0	−0.9376	1043.0	0.0758	1043.0	−0.0103
F	1096.0	1098.0	−1.4360	1096.0	0.0489	1096.0	−0.0103
AS1	1150.0	1152.0	−1.6440	1150.0	0.0035	1150.0	−0.0109
AS2	1204.0	1205.0	−1.1310	1204.0	−0.0450	1204.0	−0.0120
AS3	1258.0	1259.0	−0.3779	1258.0	−0.0813	1258.0	−0.0137
AS4	1313.0	1313.0	0.7267	1313.0	−0.0896	1313.0	−0.0154
AS5	1368.0	1367.0	2.1990	1368.0	0.0541	1368.0	−0.0167

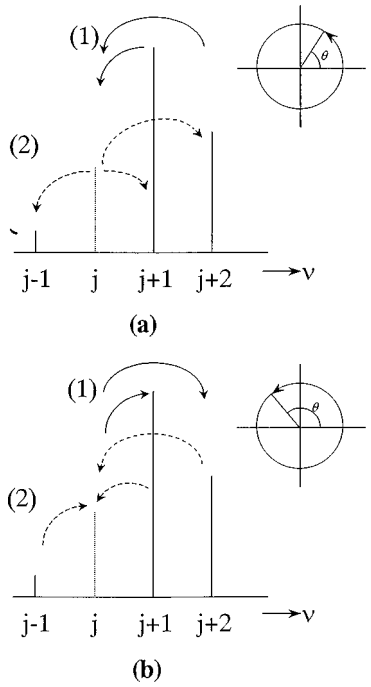

FIG. 4. Schematic explanation of energy flow in FWRM. Phase difference between the emissions interacting with each other; (a) $0-\pi/2$, (b) $\pi/2-\pi$. (1) First term, (2) second term in Eq. (3).

$$\Delta_i \equiv k_i n(\omega_i) - k_{i-1} n(\omega_{i-1}). \tag{4b}$$

The parameter $C_{j,m}$ is determined by geometry and is given by the following equation:

$$C_{j,m} = \frac{(\omega_j \omega_{j+1} \omega_m \omega_{m-1})^{1/2}}{\pi z_0 c (1 + z^2/z_0^2)(\omega_j + \omega_m)}, \tag{5}$$

where z_0 is the confocal distance. In this work, the laser is assumed to be a plane wave to simplify the calculation, and, as a result, the dispersion to a radial direction is neglected. Gain reduction by beam expansion is taken into account by the confocal parameter shown in Eq. (5). The laser beam is assumed to be focused at $z=0$, at which the gain is maximum. The first term in Eq. (3) represents the evolution of E_j from E_{j+1}, in which all the pairs of terms which affect FWRM are summarized. The second term in Eq. (3) represents the transfer of energy to E_{j-1}. These energy transfers decrease with an increase in phase mismatching, which is determined by Eq. (4). In this study, ten rotational Raman lines are assumed to be generated, i.e., $j=-4-+5$. Thus, a series of nine coupled complex differential equations require solving; the additional one is for the fundamental beam. These equations are capable of describing the complete evolution of the emission lines generated by FWRM.

III. NUMERICAL CONDITIONS

The parameters used in the numerical calculation are assumed to be similar to those obtained experimentally insofar as is possible: the pump laser wavelength is 800 nm ($\omega_f = 2.35\times10^{15}$ rad/s) which corresponds to the gain maximum of a Ti:sapphire laser; the rotational Raman shift frequency of hydrogen is 587 cm^{-1} ($\omega_R = 1.11\times10^{14}$ rad/s); the pressure of hydrogen is 1 atm; the confocal parameter z_0 is 0.6 m; the length of the Raman cell is 3 m; the initial field amplitudes of the fundamental beam and the background emission are assumed to be 1.0×10^{-1} and 1.0×10^{-30}, respectively; the gain g is 3.0×10^{-18}, which has been determined to give an intensity distribution of the Raman lines similar to that obtained experimentally [16,17]. The refractive index of 1-atm hydrogen is given by [23]

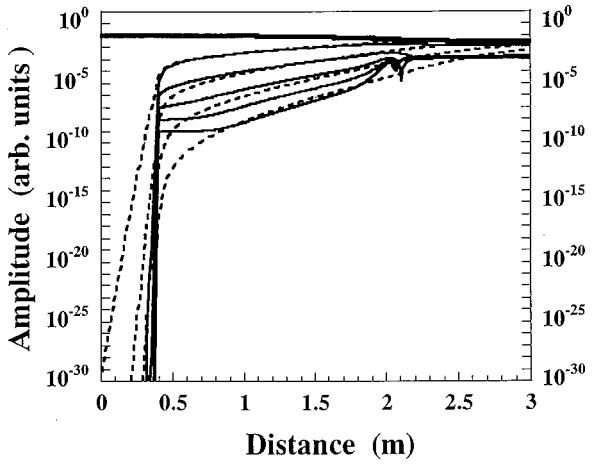

FIG. 5. Evolution of rotational Raman lines. Bold solid line: fundamental beam; dashed lines: Stokes beams; light solid lines: anti-Stokes beams. In both the cases of the Stokes and anti-Stokes beams, low-order emission lines are more efficiently enhanced than high-order ones. The sharp structures which appear at 2 m may be artifacts of computer simulation.

$$n(\omega_j) - 1 = \frac{0.919\,97\times10^{27}}{1.013\,05\times10^{31} - (\omega_j/2\pi)} + \frac{0.753\,79\times10^{27}}{1.668\,13\times10^{31} - (\omega_j/2\pi)}. \tag{6}$$

The evolutions of the high-order Stokes and anti-Stokes Raman lines were calculated by computer simulation using the Runge-Kutta-Fehlberg algorithm. In this paper, the dispersion of the cell window is neglected.

IV. RESULTS AND DISCUSSION

A. Fourier synthesis for the generation of ultrashort pulses

In the first step, high-order rotational lines are assumed to have equal intensities, i.e., a flat intensity distribution, as shown in Fig. 1; nine emission lines are assumed to be generated by passing the beam through a 3-m Raman cell. As recognized from Eqs. (2) and (3), emissions are coherently phased at $z=0$. The temporal shape of the pulse (a pulse train) is calculated by Fourier synthesis of the emission lines. The dispersion of hydrogen is taken into account, as indicated in Eqs. (3) and (4). When the dispersion was neglected, the pulse train consisted of 5-fs pulses which were repetitive at an interval of 57 fs. Due to dispersion in hydrogen, ultrashort pulses are stretched to 23 fs, as shown in Fig. 2(a). When the first-order dispersion is compensated, only the pulse train is phase shifted, while the pulse widths remain unchanged, as shown in Fig. 2(b). On the other hand, as shown in Fig. 2(c), the pulse widths can be reduced to 5 fs by

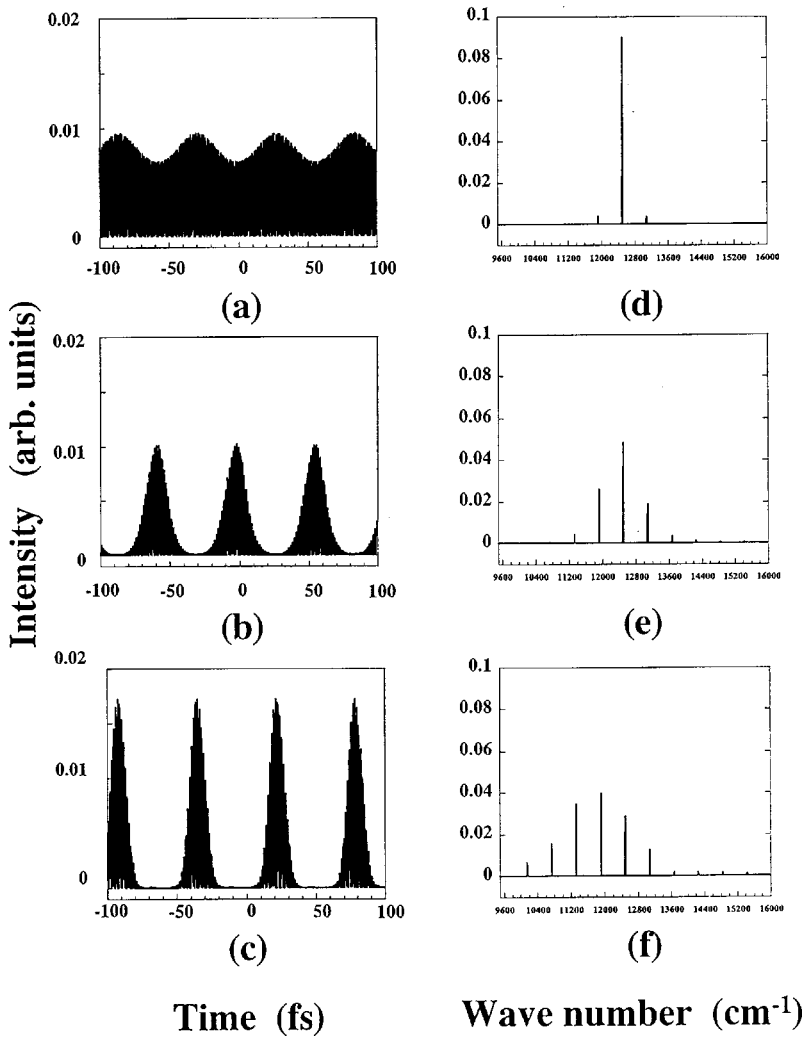

FIG. 6. Generation of ultrashort laser pulses. (a)–(c) Temporal shape, (d), (e) spectral shape; distance (z): (a), (d) 1 m; (b), (e) 2 m; (c), (f) 3 m. All the Raman waves are assumed to be phase locked at the focal point ($z=0$).

compensating the second-order dispersion. No further pulse shortening is observed even when higher-order dispersions are compensated, as shown in Figs. 2(d) and 2(e). In this case, the pulse width is apparently determined by the frequency domain of the emission lines ($587\,\mathrm{cm}^{-1}\times 9 = 5283\,\mathrm{cm}^{-1}$), and thus further pulse shortening becomes difficult without increasing the number of rotational lines generated.

Figure 3(a) shows an expanded view of Fig. 2(a); each wave of the Raman component is drawn at the bottom of the figure. Figures 3(b) and 3(c) are further expanded views of the parts corresponding to the baseline and the peak in Fig. 3(a), respectively. At the baseline, the phase of the emission lines is nearly random, and, as a result, the intensity is canceled to nearly zero. On the other hand, the waves are rather in phased in the vicinity of the peak. These results indicate that the regularity of the phases remains, even at a distance of 3 m from the beam waist.

B. Effect of dispersion

Table I shows the total phase shifts which occur when the beam travels 3 m in the Raman cell. It should be noted that the dispersion is much larger than 2π. Even the nonlinear portion of the phase shift, which is obtained by subtracting the linear portion of the dispersion, is not negligibly small. These results suggest that the phase shifts of the emission lines may be completely random and that no sharp pulse train is produced. This speculation apparently disagrees with the calculated result, i.e., a pulse train consisting of 23-fs pulses is obtained in Fig. 2(a). Therefore, an explanation is required for why a sharp pulse train is observable. In other words, it is necessary to explain (1) why the rotational lines are increased even when the phase is drastically changed (or frequently flipped from 0 to π); (2) why the phases of the emission lines are locked even though they appear to be random. A qualitative explanation is given in Fig. 4. From Eq. (3), it is possible to extract four major terms for respective summations, in which the $(j+1)$ component is assumed to be the pump beam, since the other terms provide only minor contributions in the generation of the (j) component, i.e., the Stokes beam, in the initial stage of the process because of their small intensities. For the first summation

$$E_{j+1}E_{j+1}^{*}E_{j}\quad (m=j+1),\qquad E_{j+1}E_{j+2}^{*}E_{j+1}\quad (m=j+2). \tag{7}$$

For the second summation

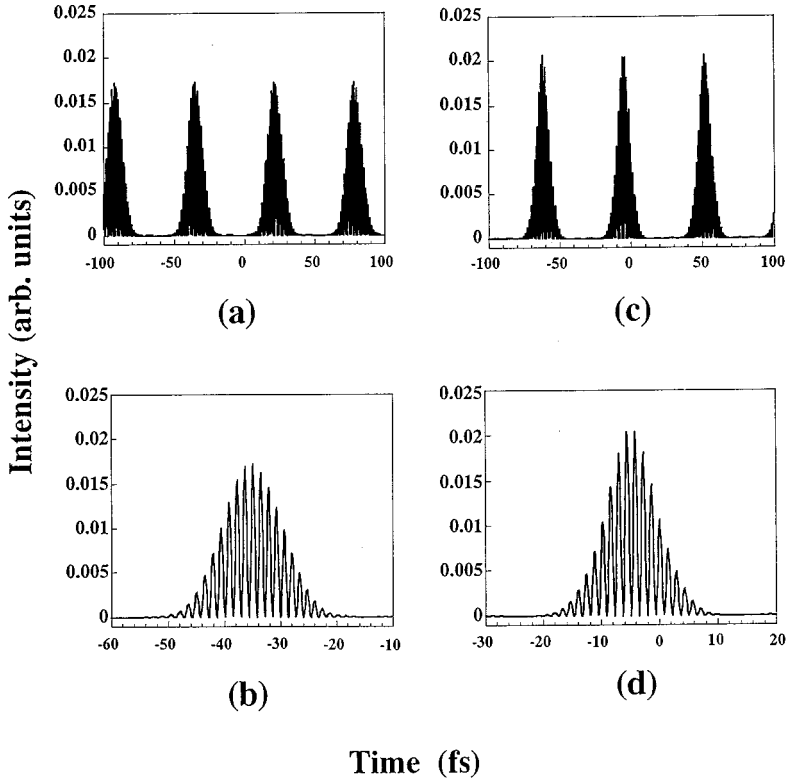

FIG. 7. Compression of the laser pulse calculated from the data shown in Fig. 6(c). Phase distortion compensation; (a) none, (c) first to second orders. (b) and (d) are the expanded views of (a) and (c), respectively.

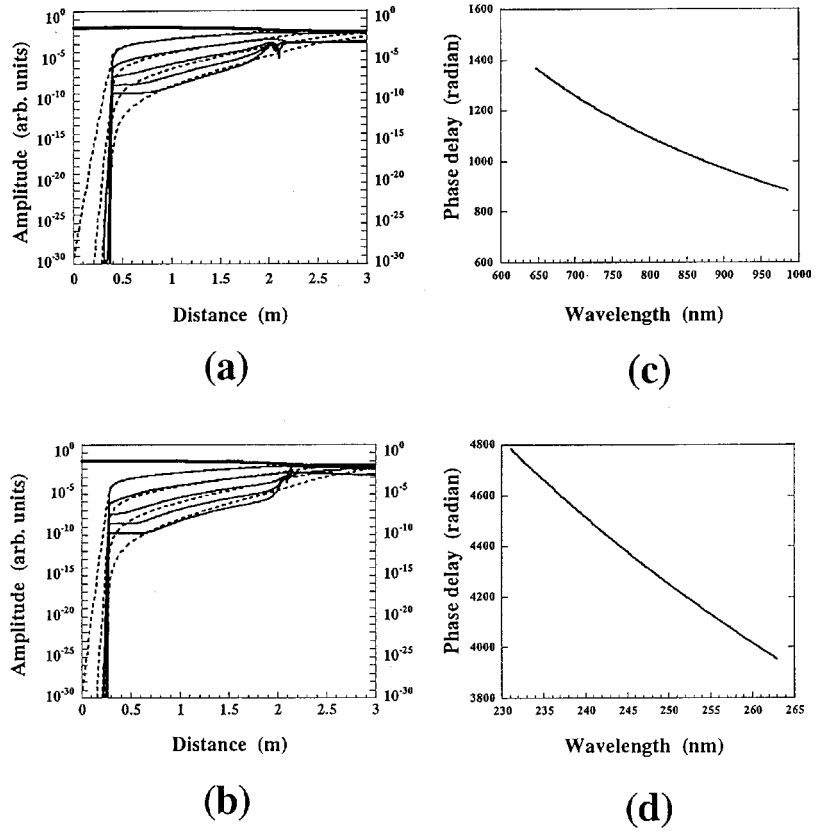

FIG. 8. Effect of laser wavelength on the evolution of rotational Raman lines. Evolution: (a) 800 nm, (b) 248 nm; dispersion: (c) 800 nm, (d) 248 nm; gain: (a) 3.0×10^{-18}, (b) 3.6×10^{-19}. In order to adjust the dispersion, the gain, e.g., the hydrogen pressure, is changed, since the difficulty of compensating for phase distortion is determined by the magnitude of the dispersion.

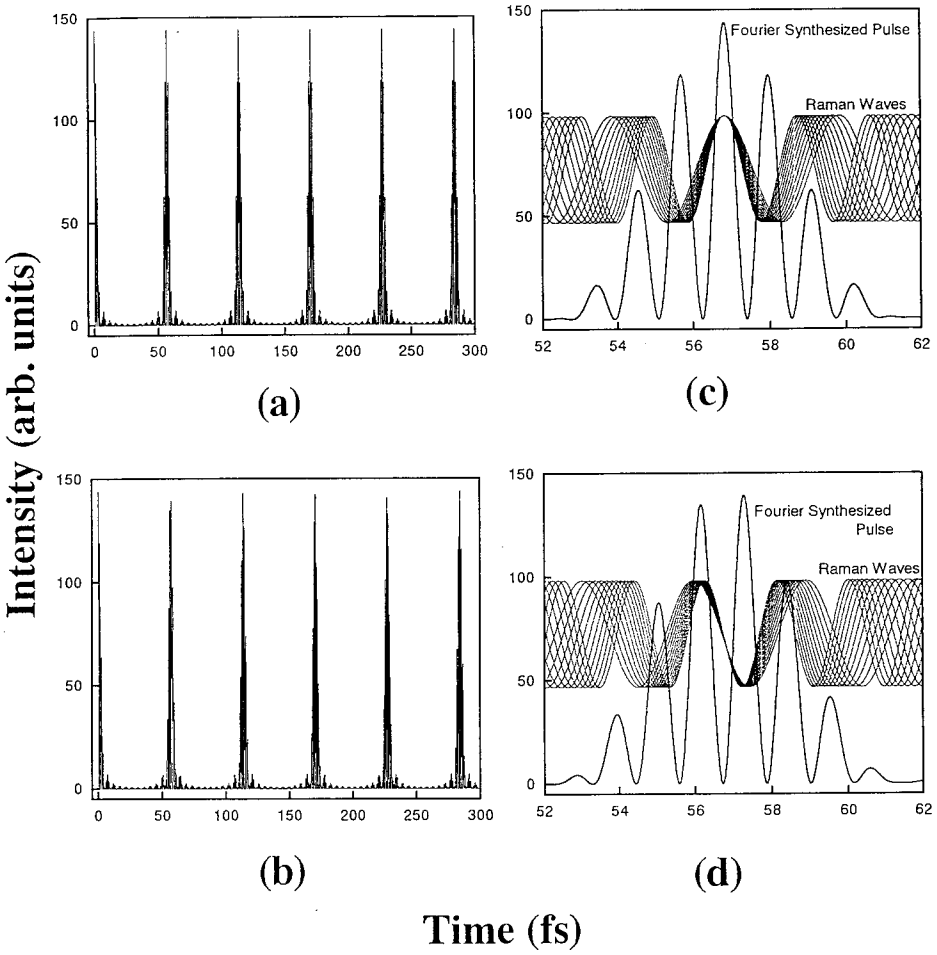

FIG. 9. Fourier synthesis of rotational Raman lines. (c) and (d) are expanded views of (a) and (b), respectively. Wavelength: (a) 811 nm, (b) 800 nm. In this calculation, 11 rotational lines are assumed to be generated simultaneously. See the caption of Table I for definition of phase delay.

$$E_{j-1}E_{j+1}^{*}E_{j} \quad (m=j+1), \qquad E_{j-1}E_{j+2}^{*}E_{j+1} \quad (m=j+2). \tag{8}$$

In the time domain from 0 to $\pi/2$ [Fig. 4(a)], the energy is transferred to the first Stokes beam mainly from the pump beam but also from the first anti-Stokes beam $(j+2)$. At the same time, the energy moves away from the first Stokes beam mainly to the fundamental (pump) beam and also to the second Stokes $(j-1)$ and the first anti-Stokes beam. In the succeeding time period which ranges from $\pi/2$ to $3\pi/2$ [Fig. 4(b)], the energy moves back from the first Stokes beam mainly to the fundamental beam and also to the first anti-Stokes beam. At the same time, the energy is transferred into the first Stokes beam mainly from the pump beam but also from the second Stokes and the first anti-Stokes beams. The enhancement of the first Stokes beam occurs again from $3\pi/2$ to 2π. As a result, the energy flows from the pump beam to high-order Stokes and anti-Stokes beams, which can be attributed to the high intensity of the pump beam and the low intensity (noise level) of the other beams. This cycle of energy transfer is repeated several hundred times over the 3-m path. It is noted that the in-phase components are strongly enhanced in the vicinity of $z=0$, and the phase shift becomes distinctive at $z>0$. The energy transfer is efficient at $z<z_0$, but the gain is still larger than unity even at $z>z_0$. These considerations explain why the energy continues to flow to high-order rotational lines even at 3 m from the beam waist, although the phase shift is much larger than $\pi/2$.

It should be noted that a phase shift of 2π does not induce any appreciable effect in the amplification of the rotational line, so long as the dispersion is linear against the frequency; the next (2π-shifted) pump wave is used to amplify the Raman wave. Thus strong enhancement may occur periodically at phase shifts of $-2n\pi$, 0, $2n\pi$, $4n\pi$,... (n, integer) for the first Stokes, the fundamental, the first anti-Stokes, the second anti-Stokes beams, . . . , respectively. Thus the in-phase components of the rotational lines are amplified efficiently even at many cycles from the beam waist so long as the dispersion is linear. It should also be noted that the linear part of the dispersion induces no appreciable effect in pulse broadening and gives only phase shifts. This explains why the pulse width cannot be compressed by compensating the first-order (linear part of) dispersion, as shown in Fig. 2(b). When the nonlinear part of the dispersion is not negligible, such a completely periodic change is not expected and the amplification then becomes nonspecific to the in-phased components and inefficient. In this case, the phases are distorted, and, as a result, the laser pulse is considerably broadened. When the nonlinear part of the dispersion is compensated, e.g., using a chirped mirror, it is possible to compress

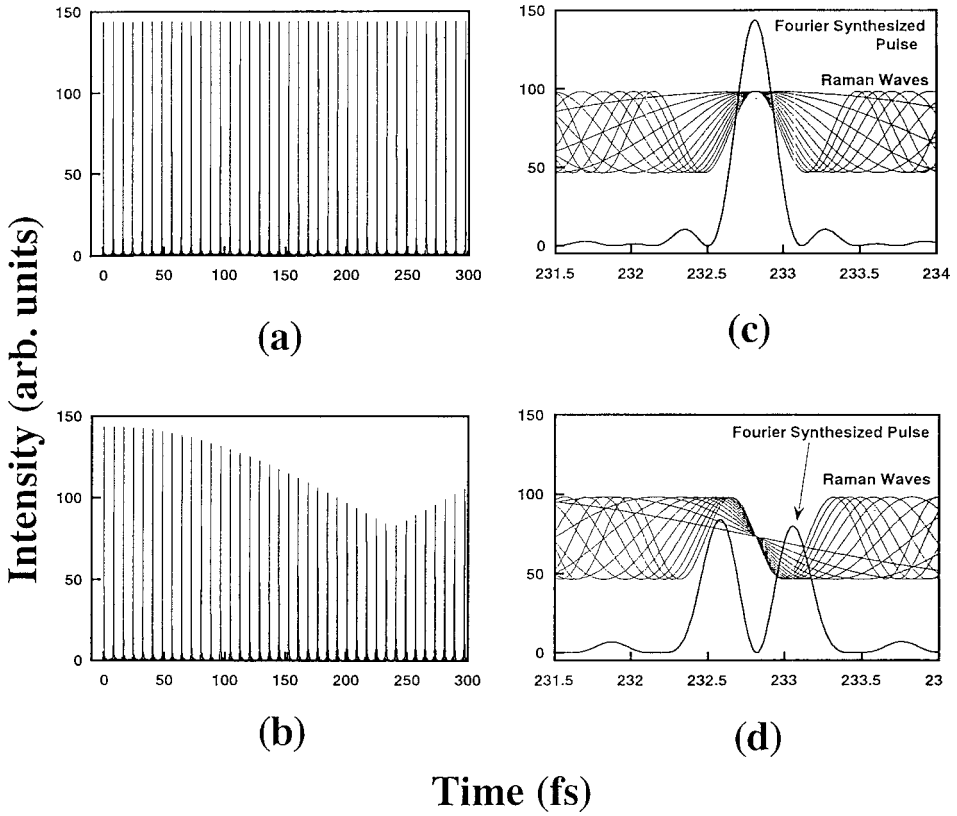

FIG. 10. Fourier synthesis of vibrational emission lines. (c) and (d) are expanded views of (a) and (b), respectively. Wavelength: (a) 802 nm, (b) 800 nm. In this calculation, 11 vibrational lines are assumed to be generated.

the laser pulse, as shown in Fig. 2(c). The pulse width is transform limited and is determined by the spectral bandwidth of the laser, i.e., the number of rotational lines. As a result, further shortening of the pulse width is difficult, unless the spectral bandwidth is expanded by increasing the number of rotational lines. Thus the capability of generating ultrashort pulses by FWRM can be attributed to a small nonlinearity of dispersion in hydrogen in the spectral region from 648 nm (fifth anti-Stokes) to 985 nm (fourth Stokes).

C. Evolution of rotational lines and generation of ultrashort pulses

In practice, it is difficult to obtain high-order rotational Raman lines with a flat intensity distribution as indicated in Fig. 1. By solving Eq. (3), it is possible to calculate the intensity distribution of the high-order Stokes and anti-Stokes lines at a specified distance from the beam waist. An example is shown in Fig. 5. All the Raman components grow rapidly within the confocal distance ($z_0 < 0.6$ m) and moderately at the end of the Raman cell. This tendency can be attributed to the consumption of the pump energy resulting from the growth of the Raman lines, to the geometry of the gradually expanding pump beam, and to the high-order (>2) distortion of the phases for the Raman lines.

The pulse shortening process is presented in Fig. 6, which also shows the spectral shapes obtained. A bell-shaped intensity distribution is obtained at the end of the Raman cell. As the Raman lines are enhanced by FWRM, the pulse train becomes sharp. In addition, the background level is reduced to zero. The dispersion also increases as the pulse train propagates 3 m in hydrogen, causing a temporal shift in the pulse train.

Because of the small nonlinear dispersion of hydrogen, the nonlinear phase shift can be easily compensated to form a transform-limited pulse using optics with small negative nonlinear dispersion. Figure 7 shows the calculated results. The pulse width is 13 fs when the dispersion is not compensated. This value remained unchanged, even when the first-order dispersion was compensated, as described. The laser pulse is compressed to 10 fs by compensating the second-order dispersion. Significant pulse shortening was not observed, even when the higher-order nonlinear dispersion was compensated. The limited capability in pulse shortening can be attributed to the nonflat intensity distribution of the Raman components, i.e., the limited spectral bandwidth of the emission lines.

D. Effect of spectral region

Two types of femtosecond lasers, i.e., a Ti:sapphire laser (800 nm) and a KrF excimer laser (248 nm), are commercially available and are used in many applications. The gain of Raman scattering is proportional to the frequency of the emission line generated. Therefore, an ultraviolet pump laser is generally useful for more efficient generation and amplification of the Raman emission. This characteristic is especially important when the other nonlinear optical phenomena such as self-focusing (SF) and SPM are competitive to the Raman and FWRM processes [17,18,24]. Moreover, a wider frequency domain is available in the ultraviolet, which is essential for the generation of several tens of attosecond

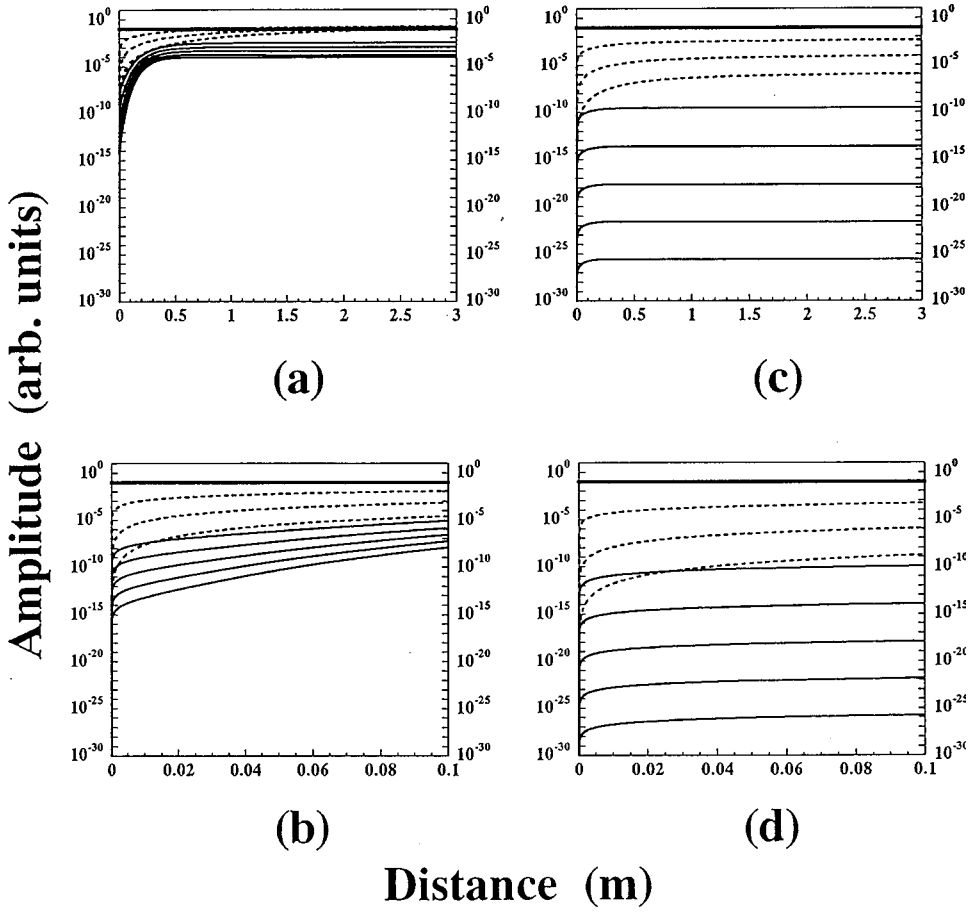

FIG. 11. Evolution of rotational Raman lines obtained by using a two-color pump beam. The gain is reduced to (a), (b) 2.4×10^{-20}; (c), (d) 1.0×10^{-21}. Scales of abscissa: (a), (c) 3 m; (b), (d) 0.1 m.

pulses. However, the dispersion is substantially increased at shorter wavelengths, especially below 300 nm, which increases the phase mismatching and reduces the amplification gain. At the same time, a large dispersion makes compensation of the phase distortion difficult. Figure 8 shows the evolution of the Raman lines, in which the gain, e.g., pressure of hydrogen, is adjusted to give similar values for phase delay. In both the cases, the Raman lines are sufficiently enhanced, indicating that both approaches can be used for the generation of ultrashort pulses. In the calculation, competition with other phenomena, such as the generation of the vibrational lines, which is more efficient in the ultraviolet, has not been taken into account. Moreover, the beam quality of the excimer laser is generally poor, which substantially increases the other nonlinear effects such as SF/SPM and suppresses the SRS/FWRM processes. For these reasons, a Ti:sapphire laser appears to be the laser of choice, although detailed experimental studies will be required to verify this conclusion.

E. Optimum laser wavelengths

For the efficient amplification of Raman lines, the phases of the pump beam and the Raman beam should be precisely superimposed at 56.82-fs ($=1/587.03\,\mathrm{cm}^{-1}\times2.9979\times10^{10}\,\mathrm{cm/s}$) intervals. For example, the r waves of the Stokes beam should travel the same distance as the $(r-1)$ waves of the fundamental beam. Since the Raman shift frequency is 587.03 cm^{-1}, the frequencies are given by

$$(q-587.03)/q=(r-1)/r, \tag{9}$$

where q is the frequency of the laser beam and r is an integer. In the spectral region of the Ti:sapphire laser, the pump beam (811.2 nm) and the Stokes beam (851.9 nm) travel 17.04 μm every 21 and 20 waves, respectively. It should be noted that an ArF excimer laser emitting at 193.5 nm can also be used for the present purpose because of coincidence with the optimum wavelength (193.6 nm). A similar calculation is performed using Eq. (10) for parahydrogen whose Raman shift frequency is 354.37 cm^{-1}.

$$(q-354.37)/q=(r-1)/r. \tag{10}$$

In this case, the wavelength of the Ti:sapphire laser requires adjusting to 806.3 nm. The emitting wavelength of the ArF laser again coincides with the optimum wavelength (193.3 nm).

The effect of wavelength mismatching is shown in Fig. 9. When the wavelength is exactly adjusted to 811.2 nm, all the Raman waves are in phased at the maximum of the peak. On the other hand, when the wavelength is shifted to 800 nm, all Raman waves are in phased at a time slightly different from the peak, i.e., the phase-locked point. The effect of wave-

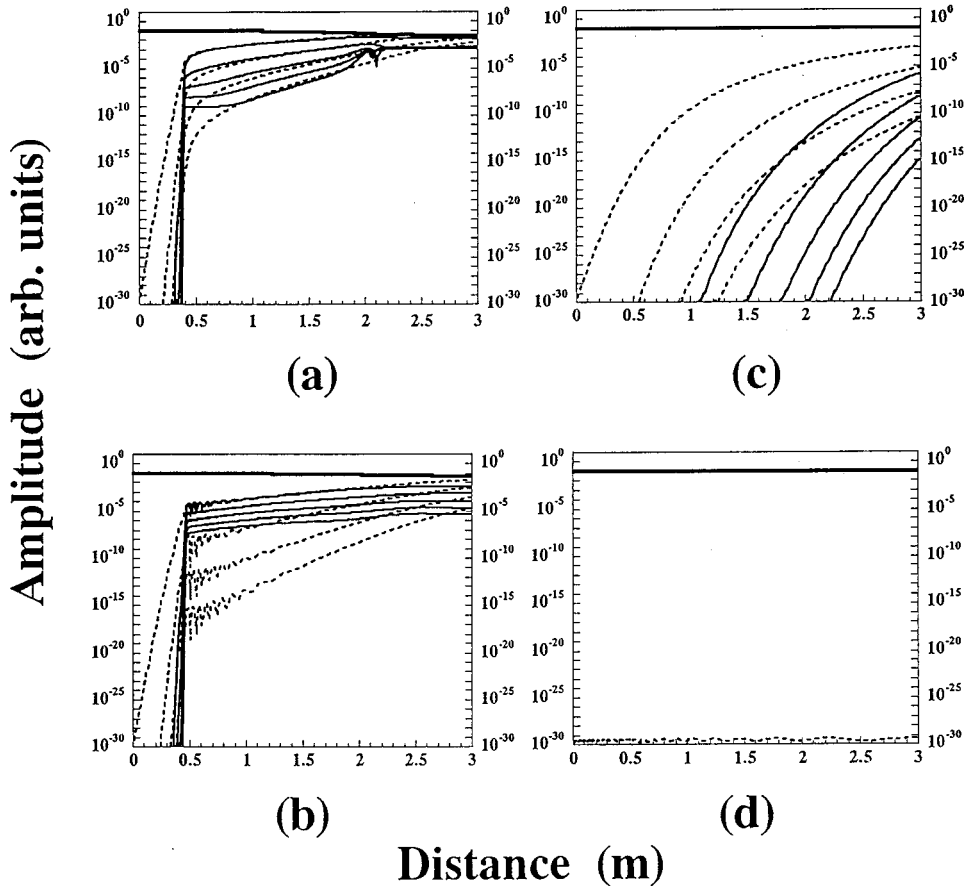

FIG. 12. Evolution of rotational Raman lines. Phase shift: (a) $0s\pi$, (b) $0.03s\pi$, (c) $0.07s\pi$, (d) $0.1s\pi$ ($s=-5, -4, -3, -2, -1$ for anti-Stokes, $s=0$ for fundamental, and $s=1, 2, 3, 4$ for Stokes lines).

length mismatching is small, when the pulse consists of several cycles of waves. However, this effect becomes serious when a shorter pulse, e.g., monocycle pulse, is generated. Figure 10 shows the calculated result, in which the generation of 11 vibrational lines is assumed. Since the wavelength range extends from the far-UV to the mid-IR, a monocycle pulse can be generated. A symmetrical monocycle pulse is obtained only when the wavelength is exactly adjusted to the optimum wavelength of 802.2 nm. When the wavelength is not optimized (800 nm), two cycles of waves appear, thus providing a stretched pulse. This wavelength matching is probably an important consideration in transient SRS and FWRM in the femtosecond regime but is less important in the nanosecond SRS and FWRM processes because of molecular collisions.

F. A two-color pump beam for the enhancement of four-wave Raman mixing

High-order rotational lines are enhanced from a noise level. A large gain (e.g., high hydrogen pressure) and a long interaction length are desirable for evolution of the rotational line, but these factors also increase the nonlinear phase shift in hydrogen. Such problems can be solved by employing a two-color pump beam to enhance FWRM. Figure 11 shows the evolution of the rotational lines obtained using a two-color pump beam whose frequencies are separated by 587 cm^{-1}. Even when the gain and the interaction length are assumed to be smaller by a factor of about 100, the intensities of the rotational lines are very rapidly and strongly enhanced from $z=0$, which is in contrast to the case of a one-color pump beam (Fig. 5). Thus a two-color pump beam is desirable, in order to minimize the hydrogen pressure and the interaction length for reduction of phase distortion, which might be especially important for the generation of ultrashort pulses less than 1 fs.

G. Phase locking in four-wave Raman mixing

A pulse train is obtained by Fourier synthesis of high-order rotational Raman emissions, whose phases are initially locked at $z=0$, as is evident from Eqs. (2) and (3). Although this model is currently used in studies of SRS and FWRM, it is necessary to investigate the validity of this assumption (phase locking at $z=0$). Figures 12 and 13 show the evolution of the rotational lines calculated by slightly changing the phases of the rotational lines at $z=0$. The efficiency in the amplification of the rotational lines is apparently reduced by increasing the phase shifts. In other words, only the noise components which are coherently phased with the fundamental beam at $z=0$ can be drastically amplified through FWRM. Such an efficient amplification of the in-phase components may be explained by the fact that the noise whose phase is exactly identical to the pump beam at $z=0$ is most efficiently enhanced exclusively as the first Stokes beam. Once the first Stokes beam is generated, the waves of the pump and the first Stokes beams have maxima at 17.0- (10 mm/587 cm^{-1}) μm intervals. Therefore, other Stokes and

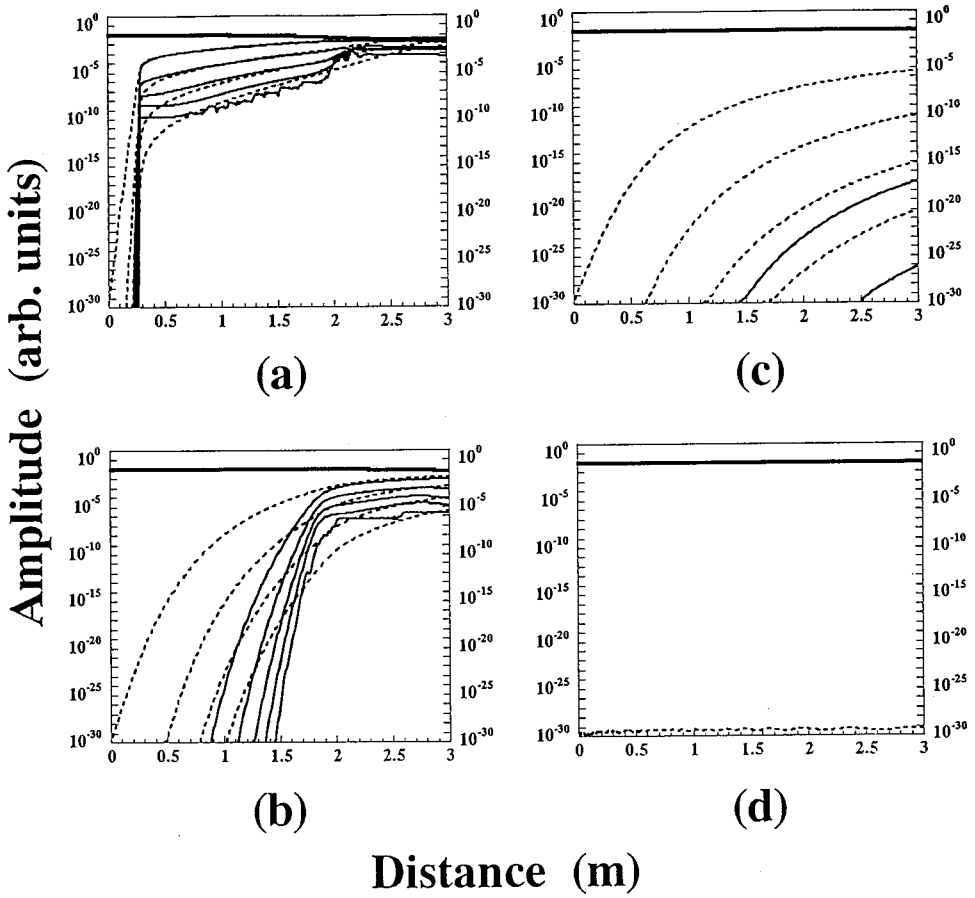

FIG. 13. Evolution of rotational Raman lines. The phase shift between the fundamental and Stokes beams is assumed to be zero at $z=0$. The phase shifts between the fundamental and other emission lines are assumed to be (a) 0π, (b) 0.38π, (c) 0.40π, (d) 0.50π.

anti-Stokes Raman components with maxima at these points are efficiently amplified. However, the wave having maxima at slightly different positions from these phase-locked points is only inefficiently amplified. This provides an explanation for why in-phase components are exclusively enhanced.

A similar calculation is performed for the experiment using a two-color pump beam and the result is shown in Fig. 14. In this case, phase-locked points are determined by the phases of the two pump waves beforehand. When no phase shift exists between the two pump beams and the generated beams, the intensities of the rotational lines are very rapidly increased, reaching nearly the same values, especially for Stokes beams. With an increase in phase shift, the rotational lines grow more inefficiently (N.B., the logarithmic scale for the ordinate). This tendency becomes more distinct when competition between the amplifications of the in-phased and nonphased components is taken into account. These considerations again indicate that Raman waves generated by FWRM are exactly phase locked at the above periodic points.

As described in the Introduction, the requirement of phase matching is well known in FWRM but phase locking (or mode locking) in FWRM is not very clear. The calculations performed in this study indicate that phase matching is equivalent to phase locking or mode locking in FWRM. In other words, the pump and generated beams are in phased; otherwise the efficiency in the generation of the Raman emission through FWRM becomes very low. This situation may be identical even in other coherent nonlinear processes such as second harmonic generation [5] and sum/difference frequency mixing.

V. CONCLUSION

In this study, high-order rotational Raman lines are strongly enhanced by FWRM and coherently phased in hydrogen, producing an ultrashort pulse train separated by 57 fs. The pulse is broadened by the phase shift which occurs as a result of nonlinear dispersion in hydrogen. The pulse is compressed by compensating the second-order term for nonlinearity, e.g., by the optics with a small negative dispersion, since the nonlinear part of the dispersion is small for gaseous hydrogen, especially in the near-infrared region.

For the generation of subfemtosecond pulses by Fourier synthesis of the Raman components, a wider frequency domain is required, which is accomplished by increasing the number of rotational lines. In fact, high-order rotational Raman lines ranging from the fourth-order Stokes (985 nm) to 40th-order anti-Stokes (278 nm) lines have already been generated experimentally even by using a chirped (nontransform-limited) 800-fs pulse in our previous research, indicating the potential generation of 0.4-fs pulses [17]. Thus the gain assumed in this study is rather conservative; (1) a low gain was, in practice, chosen in order to reduce the number of rotational lines in the calculation to reduce the time required for computer simulation; (2) a low gain, which re-

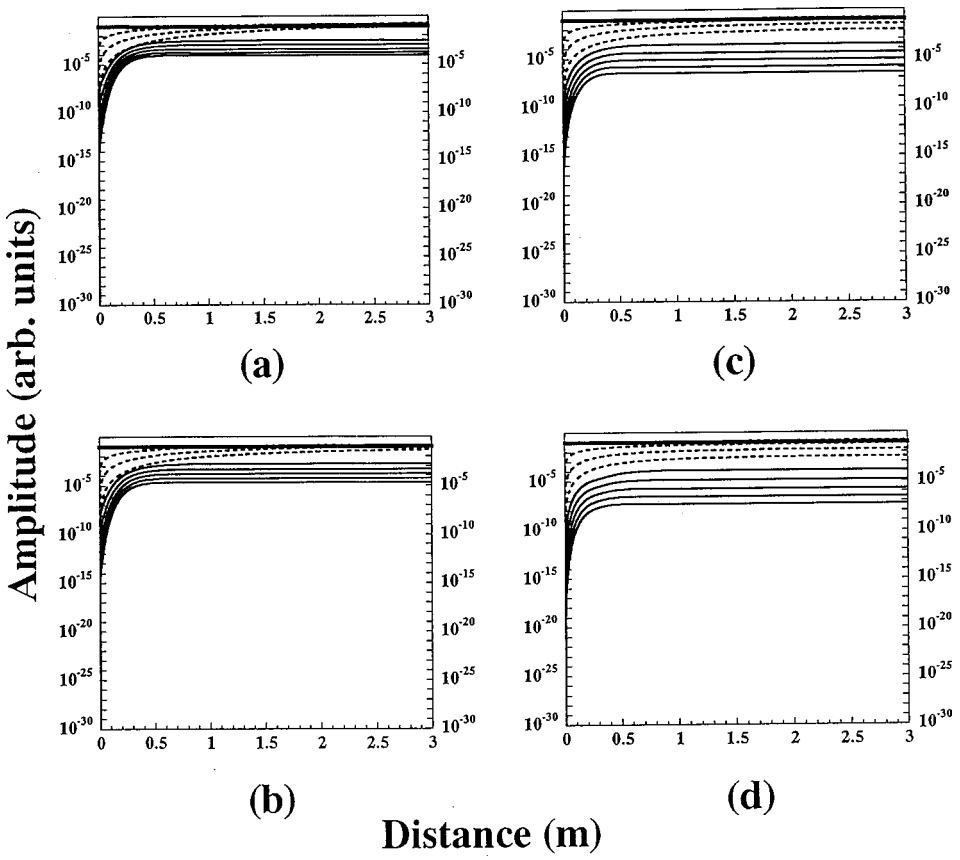

FIG. 14. Evolution of rotational Raman lines obtained by using a two-color pump beam. Gain: 2.4×10^{-20}; phase shift: (a) 0π, (b) 0.3π, (c) 0.6π, (d) 0.9π.

quires high hydrogen pressure for sufficient amplification, and a long path length are also used to enhance the effect of dispersion in hydrogen and to discuss the problems arising from these limitations. Thus, it may be possible to generate subfemtosecond laser pulses by straightforward extension of this approach, based on FWRM.

There are, however, several problems which need to be addressed in order to generate subfemtosecond optical pulses. First, the effect of dispersions induced by the Raman cell windows and even by ambient air is very serious and should be completely removed. In order to overcome this problem, injection of the hydrogen gas into a windowless gas channel placed in a vacuum chamber may be required. In this case, all experiments, including the measurements of the laser pulse width, should be performed in a vacuum chamber. Another problem may be the appreciable (not completely negligible) dispersion of pressurized hydrogen. When a picosecond pulse (e.g., 1 ps) is used as a pump beam, a comb-shaped pulse train would be observable. When a femtosecond pulse (e.g., <100-fs pulse) is used to generate a single

TABLE II. First, second, and third derivatives of phase for various optical media. Wavelength: 800 nm. The data for calculations were obtained from Ref. [25] for sapphire and fused silica and from Refs. [26] and [27] for H_2 and air, respectively.

Medium	Phase (rad)	First (rad fs)	Second (rad fs^2)	Third (rad fs^3)
Sapphire[a]	-6.912×10^4	-2.971×10^4	-290.2	-210.6
Sapphire[b]	-6.881×10^4	-2.958×10^4	-283.1	-207.0
Fused silica[c]	-5.707×10^4	-2.447×10^4	-180.8	-137.5
H_2[d]	-2.356×10^7	-1.001×10^7	-4.315	-1.998
Air[e]	-2.356×10^7	-1.001×10^7	-64.04	-29.71

[a]5 mm; ordinary wave.
[b]5 mm; extraordinary wave.
[c]5 mm.
[d]0.1 atm (the gain increases by a factor of about 100 using a two-color pump beam, allowing the hydrogen pressure to be reduced to 0.1 atm), 3 m.
[e]1 atm (atmospheric pressure), 3 m.

ultrashort pulse, a walkoff between the pump and generated beams may reduce the interaction length and then decrease the efficiency for the generation of rotational emission. Thus low hydrogen pressure and short Raman medium (e.g., by using a gas injection technique) are preferential, as long as many rotational lines can be generated. Therefore, use of efficient FWRM rather than SRS is generally preferable. This problem might also be solved by the generation of Raman solitons in a periodic nonlinear optical field for quasi-phase-matching, which may be induced by periodic phase-locked points in the propagating beam. But, in any case, the effects of residual dispersion require careful correction via the use of optics with negative group velocity dispersion. As long as the dispersion is small, it can be properly compensated, e.g., by a chirped mirror. When the dispersion is large, it is very difficult to completely compensate the nonlinear part. Generally speaking, nonlinearity may increase with increasing magnitude of dispersion. The dispersion of hydrogen is two orders of magnitude smaller than those of solid optics such as a quartz glass, thus allowing more accurate compensation of the nonlinear dispersion (see Table II). These considerations point out the potential advantage of the present method based on FWRM in hydrogen for the generation of subfemtosecond optical pulses.

ACKNOWLEDGMENT

This work was supported by a Grant-in-Aid for Scientific Research from the Ministry of Education, Science, Sports and Culture.

[1] R. L. Fork, C. H. Brito Cruz, P. C. Becker, and C. V. Shank, Opt. Lett. **12**, 483 (1987).
[2] R. L. Fork, O. E. Martinez, and J. P. Gordon, Opt. Lett. **9**, 150 (1984).
[3] A. Baltuska, Z. Wei, M. S. Pshenichnikov, and D. A. Wiersma, Opt. Lett. **22**, 102 (1997).
[4] M. Nisoli, S. De Silvestri, O. Svelto, R. Szipöcs, K. Ferencz, Ch. Spielmann, S. Sartania, and F. Krausz, Opt. Lett. **22**, 522 (1997).
[5] S. E. Harris, J. J. Macklin, and T. W. Hänsch, Opt. Commun. **100**, 487 (1993).
[6] T. W. Hänsch, Opt. Commun. **80**, 71 (1990).
[7] Gy. Farkas and Cs. Tóth, Phys. Lett. A **168**, 447 (1992).
[8] P. B. Corkum, N. H. Burnett, and M. Y. Ivanov, Opt. Lett. **19**, 1870 (1994).
[9] P. Antoine, A. L'Huillier, and M. Lewenstein, Phys. Rev. Lett. **77**, 1234 (1996).
[10] S. Yoshikawa and T. Imasaka, Opt. Commun. **96**, 94 (1993).
[11] A. E. Kaplan, Phys. Rev. Lett. **73**, 1243 (1994).
[12] A. E. Kaplan and P. L. Shkolnikov, J. Opt. Soc. Am. B **13**, 347 (1996).
[13] T. Imasaka, S. Kawasaki, and N. Ishibashi, Appl. Phys. B: Photophys. Laser Chem. **49**, 389 (1989).
[14] S. Yoshikawa, S. Kawasaki, T. Imasaka, and N. Ishibashi, Jpn. J. Appl. Phys., Part 2 **30**, L283 (1991).
[15] S. Ohtake, S. Yoshikawa, and T. Imasaka, Appl. Opt. **34**, 4337 (1995).
[16] H. Kawano, C. H. Lin, and T. Imasaka, Appl. Phys. B: Lasers Opt. **63**, 121 (1996).
[17] H. Kawano, Y. Hirakawa, and T. Imasaka, Appl. Phys. B: Lasers Opt. **65**, 1 (1997).
[18] H. Kawano, Y. Hirakawa, and T. Imasaka, IEEE J. Quantum Electron. **34**, 260 (1998).
[19] Y. Irie and T. Imasaka, Opt. Lett. **20**, 2072 (1995).
[20] F. R. Aussenegg, M. E. Lippitsch, J. Brandmüller, and W. Nitsch, Opt. Commun. **37**, 59 (1981).
[21] M. Suzuki, S. Wada, and H. Tashiro, J. Opt. Soc. Am. B **14**, 1672 (1997).
[22] P. R. Peterson, D. A. Cardimona, and A. Gavrielides, J. Opt. Soc. Am. B **4**, 1970 (1989).
[23] W. Kolos and L. Wolniewicz, J. Chem. Phys. **46**, 1426 (1967).
[24] T. Mori, Y. Hirakawa, and T. Imasaka, Opt. Commun. **148**, 110 (1998).
[25] Laser Optics and Coatings (Catalog), CVI Laser Corporation, Albuquerque, NM, USA (1997).
[26] E. R. Peck and S. Huang, J. Opt. Soc. Am. **67**, 1550 (1977).
[27] Rika Nenpyo (Chronological Scientific Tables), edited by National Astronomical Observatory, Maruzen Co., Ltd., Tokyo (1990) (in Japanese).